

line stripe and longitudinal columns are formed. By contrast, in midbrain development, *SHH* expression fans out from the ventral midline, and arcuate territories in register with the morphogen source are the result.

References and Notes

1. L. Wolpert, *J. Theor. Biol.* **25**, 1 (1969).
2. L. Wolpert, *Trends Genet.* **12**, 359 (1996).
3. J. Briscoe, J. Ericson, *Semin. Cell. Dev. Biol.* **10**, 353 (1999).
4. H. Roelink *et al.*, *Cell* **76**, 761 (1994).
5. E. Marti, D. A. Bumcrot, R. Takada, A. P. McMahon, *Nature* **375**, 322 (1995).
6. T. Sanders, A. Lumsden, C. Ragsdale, in preparation.
7. The *SHH* expression plasmid contained a cDNA encoding the 19.2-kD NH₂-terminal fragment of chick SHH [R. D. Riddle, R. L. Johnson, E. Laufer, C. Tabin, *Cell* **75**, 1401 (1993)] inserted into the expression vector pXeX [A. D. Johnson, P. A. Krieg, *Dev. Genet.* **17**, 280 (1995)]. Our results are based on whole-mount in situ hybridization analysis of 794 embryos transgenic for *SHH* expression. In 101 of the brains, *SHH* or its transcriptional target *FOXA2* (8) was de-

8. Y. Echelard *et al.*, *Cell* **75**, 1417 (1993).
9. V. Marigo, M. P. Scott, R. L. Johnson, L. V. Goodrich, C. J. Tabin, *Development* **122**, 1225 (1996).
10. Y. Watanabe, H. Nakamura, *Development* **127**, 1131 (2000).
11. T. Lecuit, S. M. Cohen, *Development* **125**, 4901 (1998).
12. J. B. Gurdon, P. Harger, A. Mitchell, P. Lemaire, *Nature* **371**, 487 (1994).
13. D. N. Keys *et al.*, *Science* **283**, 532 (1999).

14. H. F. Nijhout, *Dev. Biol.* **80**, 267 (1980).
15. K. Basler, G. Struhl, *Nature* **368**, 208 (1994).
16. B. A. Edgar, C. F. Lehner, *Science* **274**, 1646 (1996).
17. S. J. Day, P. A. Lawrence, *Development* **127**, 2977 (2000).
18. M. Placzek, J. Dodd, T. M. Jessell, *Curr. Opin. Neurobiol.* **10**, 15 (2000).
19. N. M. Le Douarin, M. E. Halpern, *Curr. Opin. Neurobiol.* **10**, 23 (2000).
20. E. A. Grove, S. Tole, J. Limon, L. Yip, C. W. Ragsdale, *Development* **125**, 2315 (1998).
21. Embryos were collected 30 min after an intravenous bromodeoxyuridine (BrdU) pulse and processed for in situ hybridization and antibody detection of BrdU-labeled cells.
22. We thank A. M. Greenlee for technical assistance, E. Ferguson, E. Grove, P. Mason, and V. Prince for discussions and C. Cepko, D. Engel, C. Goridis, M. Goulding, T. Jessell, A. Johnson, G. Martin, A. McMahon, and C. Tabin for cDNAs. Supported by National Institute of Neurological Disorders and Stroke (NIH).

26 December 2000; accepted 7 February 2001
 Published online 1 March 2001;
 10.1126/science.1058624
 Include this information when citing this paper.

Structure of an Extracellular gp130 Cytokine Receptor Signaling Complex

Dar-chone Chow,¹ Xiao-lin He,¹ Andrew L. Snow,¹ Stefan Rose-John,² K. Christopher Garcia^{1*}

The activation of gp130, a shared signal-transducing receptor for a family of cytokines, is initiated by recognition of ligand followed by oligomerization into a higher order signaling complex. Kaposi's sarcoma-associated herpesvirus encodes a functional homolog of human interleukin-6 (IL-6) that activates human gp130. In the 2.4 angstrom crystal structure of the extracellular signaling assembly between viral IL-6 and human gp130, two complexes are cross-linked into a tetramer through direct interactions between the immunoglobulin domain of gp130 and site III of viral IL-6, which is necessary for receptor activation. Unlike human IL-6 (which uses many hydrophilic residues), the viral cytokine largely uses hydrophobic amino acids to contact gp130, which enhances the complementarity of the viral IL-6-gp130 binding interfaces. The cross-reactivity of gp130 is apparently due to a chemical plasticity evident in the amphipathic gp130 cytokine-binding sites.

In vertebrates, gp130 is a shared signal-transducing receptor for a family of cytokines, including IL-6, herpesvirus IL-6 (vIL-6), IL-11, ciliary neurotrophic factor (CNTF), cardiotrophin (CT-1), leukemia inhibitory factor (LIF), oncostatin (OSM), and NNT-1/BSF3, which mediate a wide variety of both overlapping and unique biological responses in vivo (1-4). The activities of gp130 cytokines are mediated through formation of oligomeric complexes containing one or more copies of

gp130, which leads to intracellular activation of Src and Janus tyrosine kinases and of the STAT family of transcription factors (3, 5, 6).

Cytokines that activate gp130 share a common, four-helix bundle fold (7, 8). Engagement of gp130 occurs through three conserved receptor-binding epitopes on the cytokines, the third of which is unique to gp130 cytokines (9-13). By analogy to other hematopoietic cytokine receptors, gp130 is presumed to recognize ligand through its cytokine-binding homology region (CHR), located at domains 2 and 3 (D2D3) (8, 11-14). However, gp130 uniquely requires an additional NH₂-terminal (D1) immunoglobulin (Ig)-like activation domain (IGD) in order to be functionally responsive to cytokine (15).

Hematopoietic receptors such as human growth hormone (hGH) exhibit a simple ac-

tivation model characterized by the homodimerization of two receptors by one cytokine molecule via binding sites I and II (16, 17). In contrast, for gp130, "recognition" and "activation" complexes are disparate hetero-oligomeric species that are formed in a stepwise fashion (11-13, 18, 19). IL-6, the most extensively studied of the gp130 cytokines, cannot bind gp130 unless it first forms a complex with a specific α receptor (termed IL-6R α , hereafter simply R α) through a "site I" epitope (3). This binary IL-6-R α complex forms a composite epitope, termed "site II," which interacts with the CHR of gp130 (D2D3 domains) to form a trimolecular (1:1:1) recognition complex, which is not competent for signaling. A transition to a higher order signaling assembly requires recruitment of the site III epitope and IGD into the recognition complex to form the higher order activation complex (10, 15, 20, 21). Although the topology of the activated assembly remains unknown, functional studies indicate that IL-6 and IL-11 signaling complexes are "hexamers" containing two copies each of cytokine, R α , and gp130 (2:2:2) (18, 22, 23). Because the functional epitopes (sites I, II, and III) of all gp130 cytokines are in similar locations, it is likely that each signaling assembly will be constructed from a common oligomeric template.

Kaposi's sarcoma-associated herpesvirus (KSHV, or HHV8) is a recently discovered γ -herpesvirus that is a likely causative factor for the development of acquired immunodeficiency syndrome-related Kaposi's sarcoma (KS), as well as other neoplastic diseases associated with KS (24). KSHV encodes a functional homolog of interleukin-6 (termed vIL-6, 25% sequence homology) that is expressed in KS-infected cells and is able to induce angiogenesis and hematopoiesis in IL-6-dependent cell lines (25, 26). vIL-6 direct-

¹Department of Microbiology and Immunology and Department of Structural Biology, Stanford University School of Medicine, Fairchild D319, 299 Campus Drive, Stanford, CA 94305, USA. ²Department of Biochemistry, Christian-Albrechts-Universität zu Kiel, Olshausenstraße 40, D-24098 Kiel, Germany.

*To whom correspondence should be addressed. E-mail: kcgarcia@stanford.edu

REPORTS

ly activates gp130 on cells without the requirement for an α -receptor (26). Nonetheless, vIL-6 activation of gp130 initiates similar acute-phase responses and downstream signaling cascades (27). Therefore, vIL-6 is potentially a paracrine growth factor in bone marrow, suggesting a molecular mimicry in the oncogenesis of some lymphoproliferative disorders.

Here, we describe the crystal structure of KSHV IL-6 in complex with an extracellular fragment (D1D2D3) of human gp130 at 2.4 Å. This complex clarifies the structural roles of the activation epitope (site III) on the cytokine and the activation domain (IGD) on gp130, as well as the architecture of the higher order, extracellular signaling assembly. The tetrameric vIL-6-gp130 complex provides a structural template to model the hexameric extracellular signaling assemblies for other members of the gp130 cytokine family. This structure also elucidates a basis for molecular mimicry of a human cytokine by a viral homolog, and reveals the unique characteristics of gp130 that enable its extensive cross-reactivity with a diverse set of cytokines.

We coexpressed a soluble tetrameric complex (2:2) of vIL-6 and the three NH₂-terminal domains (D1D2D3) of human gp130, representing the CHR (D2D3) plus IGD (D1), in insect cells (molecular mass 126 kD) (28). Using identical methods, we coexpressed a hexameric human IL-6 (huIL-6)-R α -gp130 complex, which exhibited a 2:2:2 stoichiometry (mass 193 kD), indicating that the difference between the viral and human assemblies is the presence of the two R α in the human complex

(28). Hence, the R α independence of vIL-6, previously demonstrated in cellular experiments (26), is recapitulated with our soluble molecules. Crystallization of a nonglycosylated form of the viral complex resulted in crystals from which a complete x-ray data set to 2.4 Å was collected and the structure was determined (Fig. 1 and Table 1) (29). The crystals are space group C₂, and the complex twofold axis is coincident with a crystallographic axis (Fig. 2).

The complex assumes a tetrameric arrangement of two vIL-6 molecules and two human gp130 receptors (Fig. 2) (approximate

dimensions 95 Å by 56 Å by 65 Å). Each vIL-6 molecule bridges two different gp130 molecules, and each gp130 binds two vIL-6 molecules through structurally distinct binding epitopes. The complex is tethered through the interaction of one face of vIL-6 (site II) with gp130 (D2D3) (Figs. 2 and 3) and through a second vIL-6 epitope (site III) interacting with the D1 domain of a different gp130 (Figs. 2 and 4). The tetramer is held together entirely through ligand-specific interactions, and the D1 domain is essential for the formation of the activated, higher order

Table 1. Crystallographic statistics for the complex between vIL-6 and gp130. KSHV vIL-6 in complex with the D1D2D3 domains of human gp130 was prepared by coinfection of sf9 cells with recombinant baculovirus secretion constructs of the individual proteins (28). Nonglycosylated vIL-6 and gp130 were produced by carrying out the expression in the presence of tunicamycin, an inhibitor of N-linked glycosylation (29). The secreted complexes were harvested from the supernatant and purified by Ni-NTA, gel filtration, and anion exchange chromatography (28). The nonglycosylated complex (10 mg/ml) crystallized from 10% MPEG-2K and 0.1 M Na citrate (pH 6.5) in space group C₂, with unit cell dimensions of $a = 103$ Å, $b = 123.31$ Å, $c = 76.79$ Å, $\beta = 112.03^\circ$. A Matthews coefficient calculation (4.2 Å³/dalton) indicated a 70% solvent content for one vIL-6 and one gp130 in the asymmetric unit (45). Therefore, a half-tetramer (or half-dimer) is present in the asymmetric unit, related by C₂ symmetry to the other half of the tetramer. The crystals were flash-frozen in liquid nitrogen in the presence of mother liquor containing 20% ethylene glycol, and data sets were collected at ALS beamline 5.02 and SSRL 9-2. A single data set from a crystal that diffracted to beyond 2.4 Å was collected, and integrated and scaled using MOSFLM and SCALA, respectively (45). Initial phases for two domains of gp130 were obtained by molecular replacement with AmoRe (45) using the coordinates of the CHR (D2D3) domain of gp130 (PDB ID: 1BQU) (34). For vIL-6, only MOLREP (45) succeeded in finding a molecular replacement solution using the coordinates of huIL-6 (PDB ID: 1ALU) (37) in which the residues were truncated to alanine. No model of an Ig domain gave a satisfactory solution for the gp130 D1 domain, so the structure of the D1 domain was traced from the electron density calculated with the partial structure of the refined D2D3 and vIL-6. The entire structure was then built using XFIT, as implemented in XTALVIEW (45). The structure was refined against a maximum likelihood target function, and consisted of a rigid-body refinement, several cycles of simulated annealing with torsion angle molecular dynamics, and iterations between positional and B -factor minimization. The structure was manually rebuilt using SIGMAA-weighted $2F_{\text{obs}} - F_{\text{calc}}$ and omit $F_{\text{obs}} - F_{\text{calc}}$ maps as implemented in CNS and the graphics program O (45), and stereochemical analysis was performed with PROCHECK (45). All data between 50 Å and 2.4 Å were used, except for 5% data randomly selected for cross-validation. All residues of the receptor (2 to 302) and the body of the cytokine (6 to 172) are ordered in the electron density (residues 2 to 6 and 173 to 180 are not visible in the vIL-6 electron density). The A/B loop of vIL-6, which is often disordered in uncomplexed cytokine crystal structures, is entirely ordered and exhibits average temperature factors. No evidence of N-linked glycosylation is present on either the cytokine or the receptor.

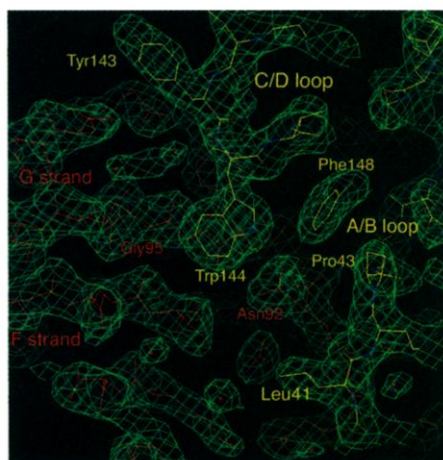


Fig. 1. Electron density in the site III interface of the vIL-6-gp130 complex. Viral IL-6 is in yellow and the gp130 D1 domain is in red. At the center of the map is vIL-6 Trp¹⁴⁴, which is at the core of the site III interface. The β -sheet strands of the gp130 D1 (F and G strands) are labeled in red. The electron density map is a SIGMAA-weighted $2F_{\text{obs}} - F_{\text{calc}}$ map at 2.4 Å contoured at 1.2σ and displayed with the program O (45).

	Data collection
Resolution (Å) (highest resolution shell)	50.0 to 2.4 (2.53 to 2.40)
Measured reflections	106,397
Unique reflections	34,376
Completeness (%)	99.0 (99.6)
R_{merge} (%)*	8.1 (48.7)
$I/\sigma(I)$	3.4 (1.4)
Mosaicity (°)	0.4
	Model refinement
Resolution range (Å)	50.0 to 2.4 (2.53 to 2.40)
R_{cryst} (%)†	21.3 (31.3)
R_{free} (%)‡	25.6 (34.6)
No. of protein atoms	3783
No. of waters	370
Average B factor (Å ²)	
Protein main chain	46.3
Protein side chain	49.8
Water	54.9
RMSD angles (°)†	0.007
RMSD bonds (Å)†	1.6
Ramachandran plot (%)	
Most favored	87.9
Allowed	12.1

* $R_{\text{merge}} = \sum_{hkl} |I - \langle I \rangle| / \sum_{hkl} I$, where I is the intensity of unique reflection hkl , and $\langle I \rangle$ is the average over symmetry-related observations of unique reflection hkl . †The RMSD in bond lengths and angles is the RMSD from the ideal stereochemical values. ‡ $R_{\text{free}} = \sum |F_{\text{obs}} - F_{\text{calc}}| / \sum F_{\text{obs}}$, where F_{obs} and F_{calc} are the observed and calculated structure factors, respectively. § R_{free} is R using a set of reflections sequestered before refinement.

assembly. The COOH-termini of each gp130 are oriented in similar directions, albeit with slightly divergent angles, where the three membrane-proximal domains not present in

this structure would lead to the cell surface, as predicted from functional studies (30, 31). As seen from the top, the overall configuration results in a large hole in the middle of the

complex (Fig. 2B) (~16 Å by 45 Å), a spacing likely critical for the gp130 extracellular domains to orient the intracellular domains correctly for signal propagation. The unused site I face of vIL-6 (B and D helices) is sterically accessible for engagement of an $R\alpha$, as would presumably occur in the human IL-6 hexamer.

The extracellular fragment of gp130, comprising the NH₂-terminal D1, D2, and D3 domains, is extended (~115 Å long) but twisted at the domain boundaries (Fig. 2). D1 is a seven-stranded β -sandwich module that adopts a noncanonical h-type Ig fold (32, 33). The gp130 D1 contains an unusual disulfide bond at its NH₂-terminus between Cys⁶ and Cys³², which tethers the A strand to the B strand. The D1 domain is linked at an approximate 45° tilt angle to the D2 domain through a proline-rich linker, which has been compared to the linker between the V and C domains of an antibody. However, unlike the flexible “elbow angle” of antibodies, the gp130 D1 forms an extensive hydrophobic interface with D2, which restricts segmental flexibility between the domains and renders the D1 domain into a fixed position.

The D2D3, or CHR, module of gp130 is composed of two β -sandwich fibronectin type III domains connected at a tilt angle of ~80° to form an elbow. The structure is similar to a previously determined crystal structure of an unliganded gp130 D2D3 (34): There are essentially no conformational differences in the exposed loops and side chains of the cytokine-binding site [root mean square deviation (RMSD) = 0.72 Å for all C α , 0.976 Å for all atoms]. Overall, gp130 appears to be a rigid structure that does not structurally adapt to cytokine, in contrast to other hematopoietic receptors that use conformational plasticity as a means of facilitating cross-reactivity (35).

The structure of vIL-6 shares the canonical up-up-down-down, ABCD four-helix bundle scaffold common to the “long chain” superfamily (Fig. 2A) (8, 36). The entire polypeptide chain is ordered in the electron density, largely as a result of packing of the A/B and C/D loops into the D1 domain of gp130 (Fig. 1) (these loops are often disordered in crystal structures of uncomplexed four-helix cytokines). Although only 25% homologous in sequence, vIL-6 most closely superimposes with huIL-6 (37), mainly because of the identical positions of two disulfide bonds (Cys³¹-Cys³⁷, Cys⁶⁰-Cys⁷⁰) and the residues comprising the helical hydrophobic core (RMSD = 1.25 Å for 82 C α , 1.7 Å total). Most of the amino acids in the hydrophobic core are conserved between human and viral IL-6. Hence, the viral cytokine has reproduced, with high fidelity, the helical scaffold on which to display alternative gp130 contact residues.

Although the structure of the huIL-6-gp130

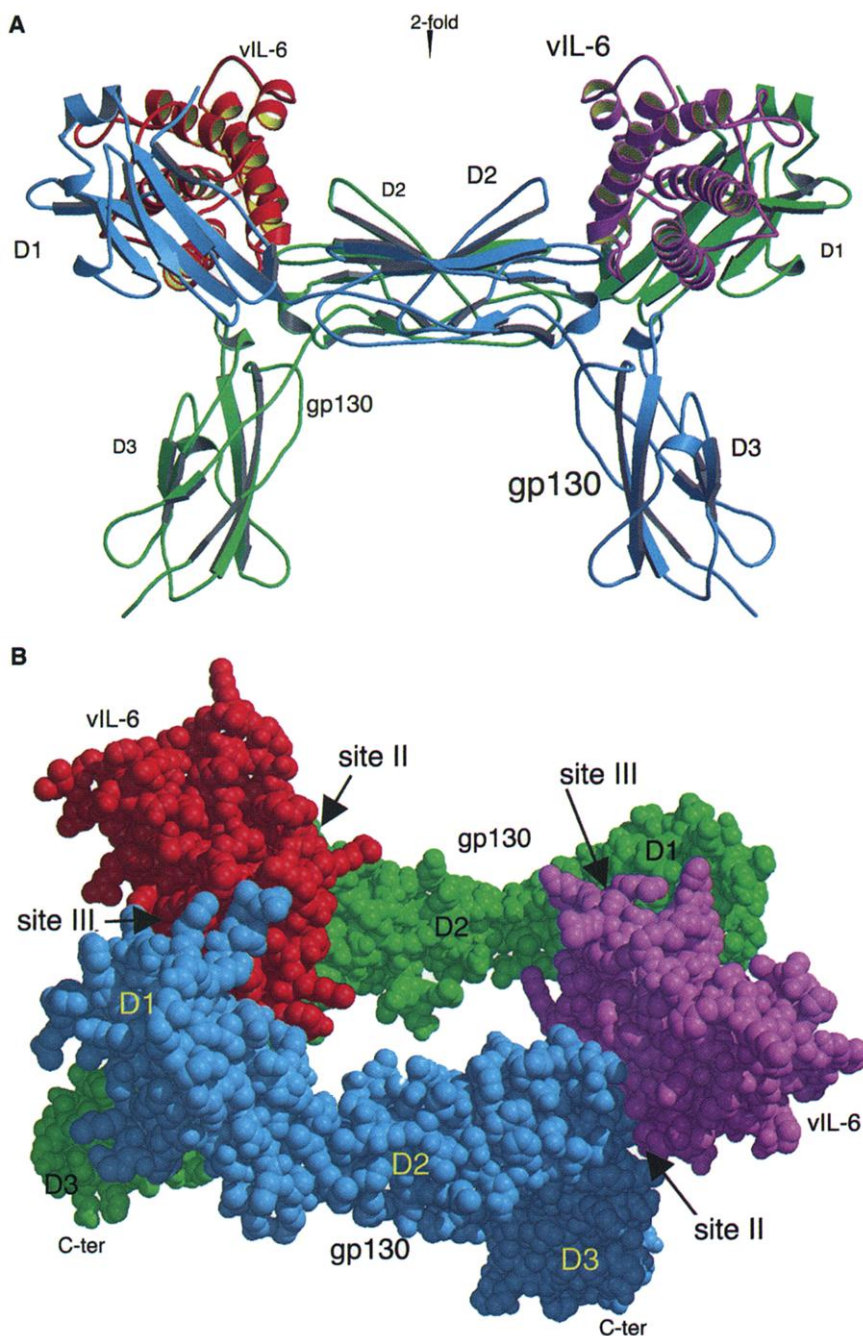


Fig. 2. Structure of the vIL-6-gp130 tetrameric signaling complex. Ribbon and space-filling models of vIL-6 complexed to gp130 (D1D2D3) in the 2:2 tetrameric oligomer are shown (gp130 molecules are blue and green, vIL-6 molecules are pink and red, and smaller and larger domain labels indicate farther and closer domains, respectively). (A) Side view of the complex; (B) a tilted view of a space-filling model. In (A), the COOH-termini of the gp130 D3 domains are at the bottom of the complex, pointing in the direction of the cell membrane. In this orientation, the second gp130 complex (in back) is obscured by the frontmost complex. When the side view is rotated toward the viewer by ~45°, the top of the complex is seen, and the second (back) receptor and cytokine from the side view (A) are now visible as related by the twofold axis, which runs through the hole in the center of the complex. The tilted view of the complex (B) enables the reader to simultaneously see the hole in the middle and the D3 domains underneath the “canopy” of vIL-6 and D1/D2 domains that dominate the uppermost portion of the complex. [Figures produced with Molscript and Raster3d (45).]

complex is not known, it is clear that both site II and site III vIL-6 epitopes use different amino acids to contact gp130 than would be used by huIL-6. However, structure-based sequence alignment between vIL-6 and huIL-6 shows that contact residues seen in the structure of the vIL-6-gp130 complex are in the same positions as huIL-6-gp130 contact residues previously mapped by mutagenesis (12). Hence, the docking orientations of the human and viral cytokines on gp130 are likely identical at both sites II and III. This allows us to make direct comparisons of amino acid positions in each cytokine with the assumption that the human gp130 cytokine and viral complex templates are identical.

The site II contact surface between vIL-6 and the gp130 CHR is primarily composed of hydrophobic interactions between the A and C helices of vIL-6 and the CD and EF loops of the D2 domain and the BC loop of the D3 domain of gp130 (Fig. 3). Thirteen vIL-6 residues and 17 gp130 contact residues bury a total of 1194 Å², with only two hydrogen bonds in the interface (38). The two hydrogen bonds (Arg¹⁵Nη2-Phe¹⁶⁹O, Asp¹⁰⁰Oδ1-Ser¹⁶⁵Oγ) may constrain the orientation of the gp130-vIL-6 crossing angle. There is excellent shape complementarity between the cytokine and receptor (Fig. 3, B and C), in which the protruding gp130 “elbow” slots into a diagonal groove on a concave face of vIL-6 created by the crossing angle of the A and C helices (Fig. 3B). A stripe of three tryptophans (Trp¹¹¹, Trp¹⁸, and Trp²¹) on vIL-6 diagonal to the cytokine helical axes (Fig. 3, B and C) defines the top, middle, and bottom of the cytokine groove and interacts, in order, with the top (CD), middle (EF), and bottom (BC) loops linking the gp130 CHR β-strand elements (Fig. 3).

The core of the interface is dominated by a hydrophobic cluster composed of Trp¹⁸ on the vIL-6 A helix (green patch in Fig. 3B, green amino acid in Fig. 3C) and Tyr¹⁶⁸-Phe¹⁶⁹ (blue patch in Fig. 4B) on the EF loop of gp130 D2, and Val²³⁰ on the BC loop of gp130 D3 (38). The vIL-6 Trp¹⁸ and gp130 Phe¹⁶⁹ protrude into mutually complementary pockets (Fig. 3, B and C). Mutation of gp130 Phe¹⁶⁹ and Val²³⁰ is disruptive to interaction with gp130 cytokines, and large aromatics at gp130 positions 168 and 169 are highly conserved across species (31, 34, 39). Hence, the insertion of the receptor Phe¹⁶⁹ into a pocket on the cytokine A/C face likely represents a common feature underlying gp130 cytokine recognition. These amino acids, then, may represent the energetic “hotspots” of the site II interface, as has been observed for a structurally analogous Trp residue (Trp¹⁰⁴) in the core of the hGH receptor interface (40).

None of the 13 vIL-6 site II residues in contact with gp130 are shared with huIL-6. The stripe of three tryptophans on vIL-6 (Trp¹⁸, Trp²¹, and Trp¹¹¹) is replaced by

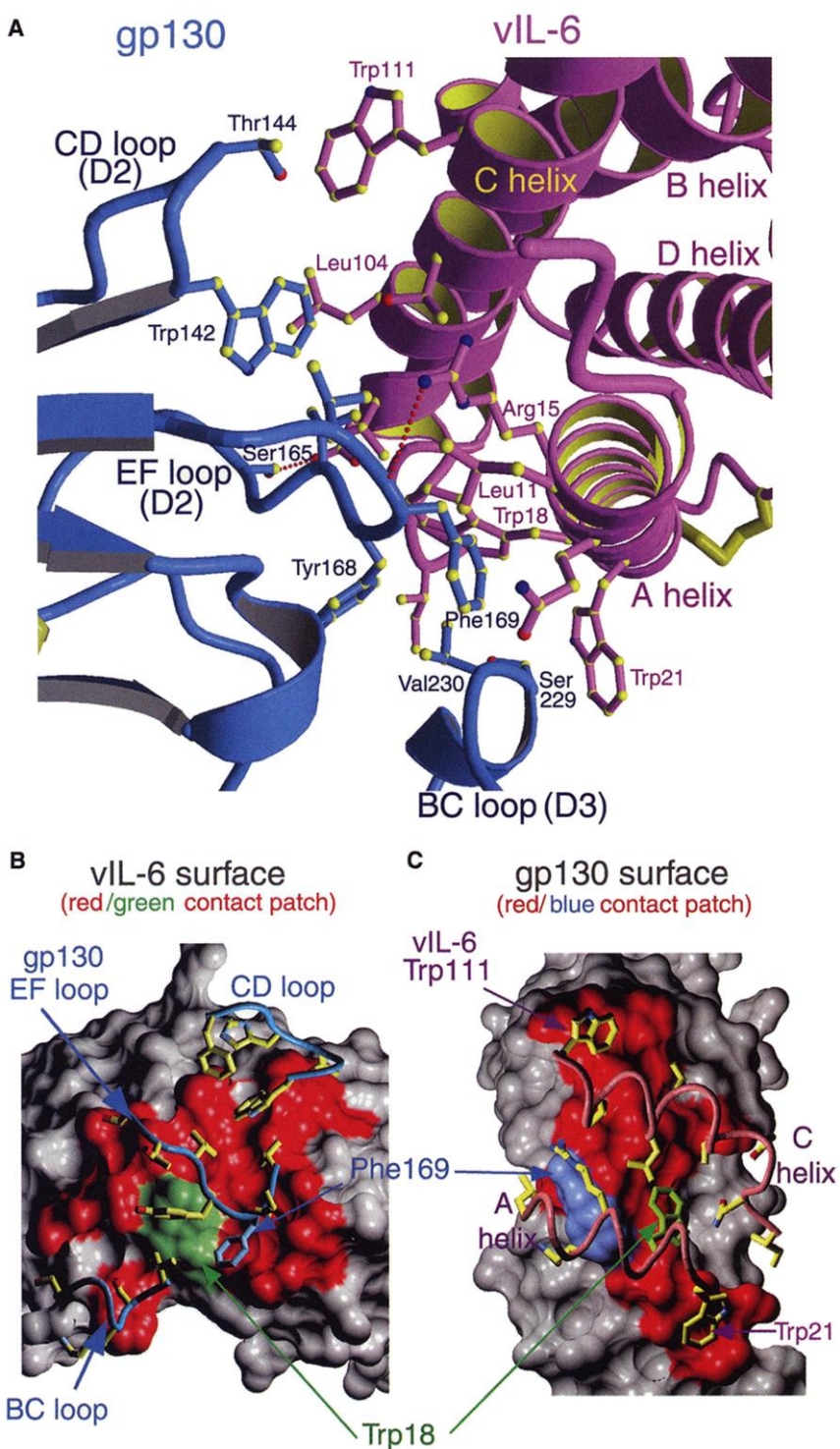


Fig. 3. Molecular anatomy and shape complementarity of the site II interface. (A) Amino acid contact residues within the site II interface; gp130 (blue) is at the left and vIL-6 (purple) at the right, and hydrogen bonds appear as red dotted lines. The conserved gp130 Phe¹⁶⁹ and vIL-6 Trp¹⁸ are in the center of the interface. (B and C) The site II vIL-6-gp130 interface is peeled open, and the contact residues of one molecule are projected onto the buried surface (red) of the interacting protein. Trp¹⁸ of vIL-6 (green) and Phe¹⁶⁹ of gp130 (blue) are used as anchor points (arrows) to orient the reader between the two surfaces. In (B), the gp130 contact residues (yellow) and binding-site loops (blue) are shown as sticks projected onto the molecular surface of vIL-6, where the buried portion is highlighted in red. A deep canyon that receives the protruding gp130 elbow is evident on the surface of vIL-6. The central Trp¹⁸ of vIL-6 is highlighted on the red surface as a green patch. In (C), the vIL-6 contact residues (yellow) and helices (pink) are drawn as sticks projected onto the protruding molecular surface of gp130. The Phe¹⁶⁹ of gp130 is drawn as a blue patch [see (38)]. [Figures produced with Molscript, Raster3d, and VMD (surface calculated with MSMS using 1.4 Å probe radius) (45).]

Tyr³¹, Asp³⁴, and Gln¹²⁴, respectively. Hence, the three largest hydrophobic contact residues in vIL-6 are replaced by smaller, more polar amino acids in huIL-6, which would reduce the shape complementarity of

this interface and rationalizes, in part, the huIL-6 requirement for its α -receptor ($R\alpha$) to stabilize binding to a nonoptimal gp130 D2D3 binding site. The increased size, hydrophobicity, and shape complementarity of

key contact positions in vIL-6 site II renders an $R\alpha$ dispensable.

The molecular basis of the striking cross-reactivity of gp130 for a diverse set (15 to 20% sequence homology) of cytokines likely resides in a combination of highly solvent-exposed hydrophobic residues in the gp130 CHR binding site (Fig. 3, A and B) and an amphipathic binding surface capable of both nonpolar and polar interactions. The solvent accessibility of nonpolar residues on the surface of the gp130 site II implies a favorable entropic driving force for shielding this surface from solvent through burial by cytokine, and the lack of side chain-specific polar interactions may lead to promiscuity, as has been suggested for the binding site of human Ig-Fc (41). The cross-reactivity of gp130 is further enhanced by the amphipathic nature of the site II and III surfaces, which enables the accommodation of a spectrum of binding chemistries.

All gp130 cytokines possess a third (site III) functional epitope, which is necessary for receptor activation, but the nature of its interaction with gp130 has been unclear (10, 13). In the structure of the vIL-6-gp130 complex, the site III interaction comprises an extensive interface between the tips of the vIL-6 four-helix bundle (A/B loop and start of D helix) and the edge (G and F strands) of the upper three-stranded β sheet of the gp130 IGD (D1) domain (Figs. 1 and 4) (38). The complementary shape of the interface is formed by the convex tip of vIL-6 resting in a depression formed by the curvature of the upper D1 β sheet (Fig. 4, A and C). The interface is discontinuous and is composed of two separate structural elements on vIL-6: residues in the A/B loop (site IIIa) and the start of the D helix (site IIIb) (Fig. 4) (38). These loops primarily interact with the G β strand, and to a lesser extent with the F, A, and c' strands of the receptor D1 Ig β sandwich (Fig. 1). This region of an Ig domain has not been previously seen as a ligand-binding site. A total of 1641 \AA^2 of surface is buried in the interface and is partitioned on vIL-6 into 60% from the A/B loop (site IIIa) and 40% from the D helix (site IIIb) (38). The core of the interface is formed by vIL-6 site IIIb hydrophobic residues Tyr¹⁴³, Trp¹⁴⁴, and Phe¹⁴⁸ packing into a depression on the surface of the G strand. In site IIIa, the vIL-6 A/B loop, usually disordered in uncomplexed cytokines, forms an almost continuous interaction with D1 through numerous main-chain H-bonds (Fig. 4A). The NH₂-terminal four residues of D1, which precede the unusual disulfide (Cys⁶-Cys³²) between strands A and B, form a strand-like interaction with A/B loop residues 44 to 49 of vIL-6 (Fig. 4A). Although the functional importance of this contact is unknown, modifications to the NH₂-terminus of gp130 disrupt signaling (42).

Extensive mutagenesis data on gp130 cyto-

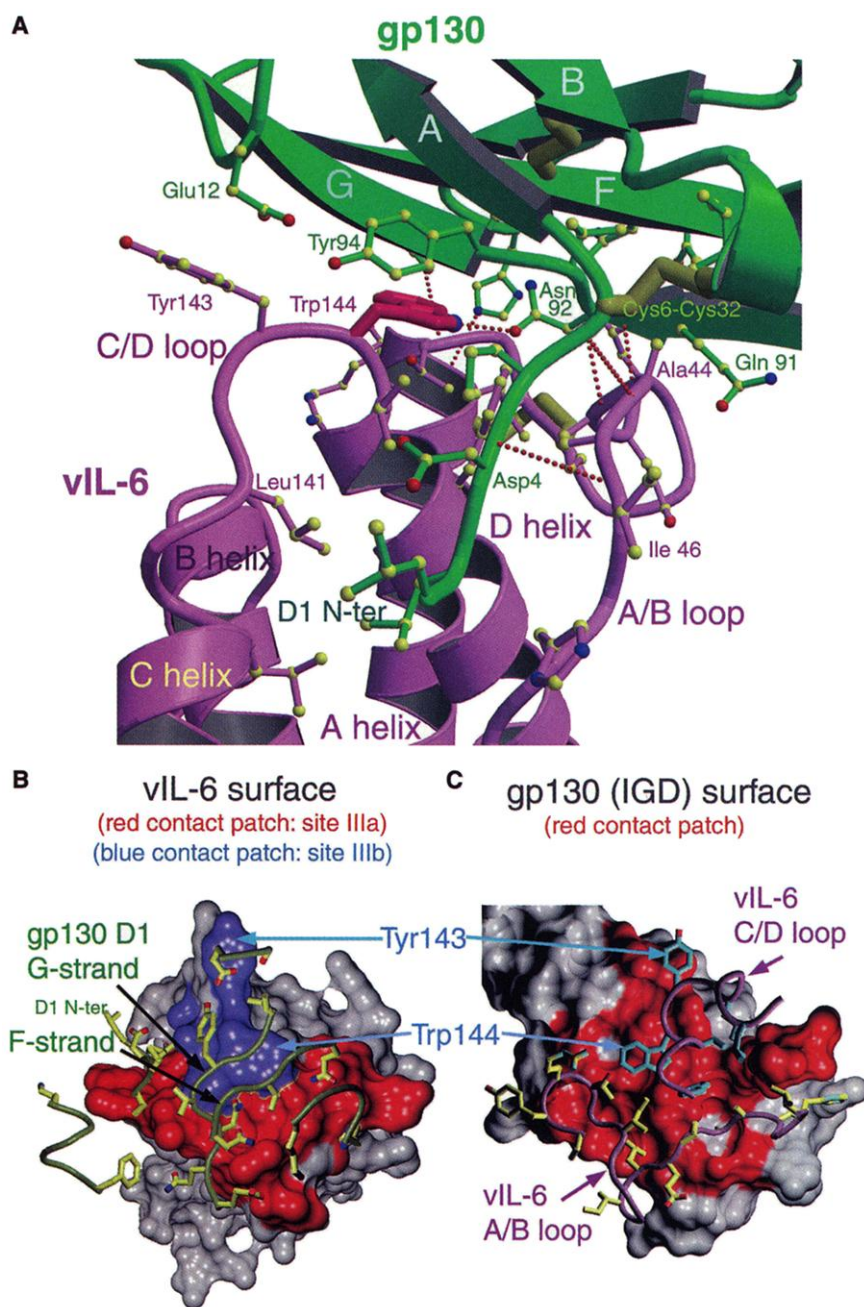


Fig. 4. Molecular anatomy and shape complementarity of the site III interface. (A) Amino acid contact residues within the site III interface; vIL-6 (magenta) is at the bottom and the gp130 D1 (IGD) domain (green) at the top, and hydrogen bonds appear as red dotted lines. The hallmark site III residue of vIL-6, Trp¹⁴⁴, is drawn in purple with a thicker stick rendering. β -sheet strands of the gp130 IGD are labeled as indicated. (B and C) The site III vIL-6-gp130 interface is peeled open, and the contact residues of one molecule are projected onto the buried surface (red) of the interacting protein. Tyr¹⁴³ and Trp¹⁴⁴ of vIL-6 are used as anchor points (blue arrows) to orient the reader between the two surfaces. In (B), the vIL-6 contact residues (yellow for site IIIa, blue for site IIIb) and binding-site loops are shown as sticks projected onto the molecular surface of the gp130 IGD where the buried portion is highlighted in red. In (C), the gp130 IGD contact residues (yellow) and β -sheet strands (green) are drawn as sticks projected onto the protruding site III molecular surface of vIL-6. The total site III contact surface of vIL-6 is divided into site IIIa (red) and site IIIb (blue) to indicate the relative locations of side chains within the surface. The strand designations of the IGD β -sheet strands are labeled.

kines implicate a large hydrophobic residue at the NH₂-terminus of the D helix as being critical to a functional site III (9, 10, 18, 43). In particular, a critical Trp¹⁵⁷ in huIL-6 (Phe¹⁶⁰ in OSM, CNTF, and LIF) is present at the identical position (Trp¹⁴⁴) in the vIL-6 structure, placing it in the center of the interface (Figs. 1 and 4), where it buries the largest fraction of surface area of all residues in site III and forms a hydrogen bond with Asn⁹² of D1 (38). Hence, the vIL-6 molecular mimicry of the huIL-6 site III is achieved through preservation of an identical central core residue (Trp¹⁴⁴) that likely is the "hotspot" of the interface, but a different set of peripheral contact residues is presented (9 of 13 vIL-6 contact residues differ).

The site III binding region on the gp130 D1 contains both degenerate and specific structural features relevant to its function as a shared signal transducer. D1 is a rigid structural framework that does not appear to use conformational plasticity to cross-react with multiple different cytokine site III surfaces. Rather, the site III interaction surface of the cytokine is composed primarily of flexible interhelical loops, and it appears to adapt its structure to the surface of D1 in an induced-fit type of interaction. The predominance of main-chain H-bonds between the A/B loops (site IIIa) and D1 also enhances the promiscuity of the site III-D1 interface (Fig. 4). Similar to site II, the D1 binding site uses amphipathicity to broaden the range of ligand surface chemistries with which it can interact, with residues such as Tyr⁹⁴ and Asn⁹² participating in both polar and nonpolar interactions (the gp130 binding surface is 58% polar, 42% nonpolar; the vIL-6 buried surface is 16% polar, 84% nonpolar).

Our biochemical studies using a soluble D1D2D3 fragment of gp130 indicate that the human IL-6 signaling assembly consists of a "hexamer" containing two huIL-6, two R α , and two gp130 (2:2:2), which is consistent with data from functional studies using full-length receptor (18, 22, 23, 44). In the structure of the vIL-6-gp130 tetramer, the outward helical face of vIL-6 (B and D helices), where huIL-6 would interact with R α (site I), is unoccupied but is openly accessible in the complex (Fig. 2), clarifying the location of R α in the human signaling complexes. For the huIL-6 hexamer, the two site I faces will likely each be occupied by an R α in a manner similar to the site I interaction between hGH and GHR, creating the hexameric structure. This hexamer model directly applies to human IL-11 and IL-12 signaling complexes, as they both dimerize shared signal transducers. The resolution of how gp130 cytokines such as LIF, CNTF, OSM, and CT-1 heterodimerize their receptors, breaking the hexameric symmetry, remains a challenge for future structural studies of this important cytokine superfamily.

References and Notes

1. M. Hibi *et al.*, *Cell* **63**, 1149 (1990).
2. T. Kishimoto, T. Taga, S. Akira, *Cell* **76**, 253 (1994).
3. T. Taga, T. Kishimoto, *Annu. Rev. Immunol.* **15**, 797 (1997).
4. G. Senaldi *et al.*, *Proc. Natl. Acad. Sci. U.S.A.* **96**, 11458 (1999).
5. J. N. Ihle, B. A. Witthuhn, F. W. Quelle, K. Yamamoto, O. Silvennoinen, *Annu. Rev. Immunol.* **13**, 369 (1995).
6. P. C. Heinrich, I. Behrmann, G. Muller-Newen, F. Schaper, L. Graeve, *Biochem. J.* **334**, 297 (1998).
7. J. F. Bazan, *Immunol. Today* **11**, 350 (1990).
8. S. R. Sprang, J. F. Bazan, *Curr. Opin. Struct. Biol.* **3**, 815 (1993).
9. J. Brakenhoff *et al.*, *J. Biol. Chem.* **269**, 86 (1994).
10. M. Inoue *et al.*, *Proc. Natl. Acad. Sci. U.S.A.* **92**, 8579 (1995).
11. J. Grotzinger, G. Kurapkat, A. Wollmer, M. Kalai, S. Rose-John, *Proteins* **27**, 96 (1997).
12. R. J. Simpson, A. Hammacher, D. K. Smith, J. M. Matthews, L. D. Ward, *Protein Sci.* **6**, 929 (1997).
13. J. Bravo, J. K. Heath, *EMBO J.* **19**, 2399 (2000).
14. J. F. Bazan, *Proc. Natl. Acad. Sci. U.S.A.* **87**, 6934 (1990).
15. A. Hammacher *et al.*, *J. Biol. Chem.* **273**, 22701 (1998).
16. J. A. Wells, A. M. de Vos, *Annu. Rev. Biochem.* **65**, 609 (1996).
17. I. A. Wilson, L. K. Jolliffe, *Curr. Opin. Struct. Biol.* **9**, 696 (1999).
18. G. Paonessa *et al.*, *EMBO J.* **14**, 1942 (1995).
19. D. Staunton, K. R. Hudson, J. K. Heath, *Protein Eng.* **11**, 1093 (1998).
20. I. Kurth *et al.*, *J. Immunol.* **162**, 1480 (1999).
21. K. J. Kallen *et al.*, *J. Biol. Chem.* **274**, 11859 (1999).
22. L. D. Ward, G. J. Howlett, A. Hammacher, R. L. Moritz, R. J. Simpson, *Ann. N.Y. Acad. Sci.* **762**, 471 (1995).
23. V. A. Barton, M. A. Hall, K. R. Hudson, J. K. Heath, *J. Biol. Chem.* **275**, 36197 (2000).
24. E. Cesarman, Y. Chang, P. S. Moore, J. W. Said, D. M. Knowles, *N. Engl. J. Med.* **332**, 1186 (1995).
25. P. S. Moore, C. Boshoff, R. A. Weiss, Y. Chang, *Science* **274**, 1739 (1996).
26. S. H. Hoischen *et al.*, *Eur. J. Biochem.* **267**, 3604 (2000).
27. J. Molden, Y. Chang, Y. You, P. S. Moore, M. A. Goldsmith, *J. Biol. Chem.* **272**, 19625 (1997).
28. The proteins and complexes for these studies were produced using the baculovirus system in insect cells (Baculogold-Pharmingen). We amplified and subcloned the D1D2D3 domains of gp130 (amino acid residues 2 to 303) and the mature coding sequence of KSHV IL-6 (residues 2 to 180) into the pAcgp67A secretion vector (Pharmingen); 6-histidine tags were appended to the COOH-termini. Sf9 cells were transfected and recombinant virus was amplified using standard methods. For large-scale expression of the complexes, Tn5 cells grown to a density of 2×10^6 cells per milliliter in Insect-Xpress (BioWhittaker) in a shaking Fernbach flask were simultaneously infected with recombinant virus from both gp130 and vIL-6 at a multiplicity of infection of at least 10. Coinfection substantially increased the yield of complex versus expression of each individual component and subsequent mixing. Cultures were allowed to progress for 48 to 60 hours before the cells were pelleted by centrifugation, the supernatant was clarified by filtration, and the volume of the supernatant was reduced by tangential flow concentration. The complexes were captured by Ni-NTA resin and then purified by gel filtration chromatography (Superdex-200) and/or mono-Q fast protein liquid chromatography (Pharmacia). The vIL-6 and gp130 formed a stoichiometric, stable complex whose mass was determined by gel filtration and analytical ultracentrifugation to be ~126 kD (theoretical mass, 131.5 kD). This mass indicates the presence of a 2:2 ratio of gp130 to vIL-6. Human IL-6-R α and gp130 formed an equally stable complex of ~193 kD, indicating a 2:2:2 stoichiometry (theoretical mass, 191.6 kD) (D. C. Chow *et al.*, unpublished data). The mass difference between the vIL-6-gp130 and huIL-6-R α -gp130 complexes (~60 kD) is accounted for by the 2 R α ($2 \times \sim 30$ kD) not present in the vIL-6 complex.
29. The complexes expressed from insect cells are heavily glycosylated. The gp130 D1D2D3 domains contain six potential N-linked glycosylation sites, and the vIL-6 contains two. Our enzymatic deglycosylation experiments indicate that all sites are used for carbohydrate addition. We crystallized the fully glycosylated complex; however, these crystals, although ordered, failed to diffract x-rays beyond 8 to 9 Å at synchrotron x-ray sources. Therefore, we expressed the complex in the presence of a known N-linked glycosylation inhibitor, tunicamycin. Addition of tunicamycin (0.2 µg/ml) to the expression media immediately before infection resulted in the production of complexes free of N-linked carbohydrate. This material was purified by methods identical to those used for the glycosylated material, and in all respects it behaved identically to the glycosylated complex. We grew crystals of this material that diffracted x-rays to beyond 2.0 Å resolution, and from which a complete 2.4 Å data set was collected.
30. A. Hammacher *et al.*, *Biochem. J.* **345**, 25 (2000).
31. I. Kurth *et al.*, *J. Immunol.* **164**, 273 (2000).
32. The D1 domain of gp130 can be classified as an h-type Ig domain according to the classification criteria of Bork (33). There is a 4-on-3 sheet arrangement of the order a-b-e-d on c-c'-f-g. Although there is a short c' strand, which would place it in the v-type fold, there are only 12 amino acids between the start of the c strand and the start of the e strand, placing it in the h-type category. A DALI search of the D1 resulted in the highest Z-scores for both v- and h-type Ig folds [L. Holm, C. Sander, *J. Mol. Biol.* **233**, 123 (1993)]. Hence, the gp130 D1 is best considered a hybrid of a v- and h-type Ig fold, with a short c-c' strand.
33. P. Bork, L. Holm, C. Sander, *J. Mol. Biol.* **242**, 309 (1994).
34. J. Bravo, D. Staunton, J. K. Heath, E. Y. Jones, *EMBO J.* **17**, 1665 (1998).
35. S. Atwell, M. Ultsch, A. M. De Vos, J. A. Wells, *Science* **278**, 1125 (1997).
36. J. F. Bazan, *Neuron* **7**, 197 (1991).
37. W. Somers, M. Stahl, J. S. Seehra, *EMBO J.* **16**, 989 (1997).
38. See Science Online (www.sciencemag.org/cgi/content/full/291/5511/2150/DC1).
39. U. Horsten *et al.*, *J. Biol. Chem.* **272**, 23748 (1997).
40. T. Clackson, J. A. Wells, *Science* **267**, 383 (1995).
41. W. L. DeLano, M. H. Ultsch, A. M. de Vos, J. A. Wells, *Science* **287**, 1279 (2000).
42. R. L. Moritz *et al.*, *Growth Factors* **16**, 265 (1999).
43. M. C. Deller *et al.*, *Struct. Fold Des.* **8**, 863 (2000).
44. D. C. Chow *et al.*, unpublished data.
45. Crystallographic and graphics programs used were ALS-CRIP [G. J. Barton, *Protein Eng.* **6**, 37 (1993)]; CCP4, AmoRe, MOSFLM, SCALA [CCP4, *Acta Crystallogr.* **D50**, 760 (1994)]; MOLREP [V. Vagin, A. Teplyaev, *J. Appl. Crystallogr.* **30**, 1022 (1997)]; XTALVIEW (XFIT) [D. E. McRee, *J. Struct. Biol.* **125**, 156 (1999)]; CNS [A. T. Brünger *et al.*, *Acta Crystallogr.* **D54**, 905 (1998)]; MOLSCRIPT [P. J. Kraulis, *J. Appl. Crystallogr.* **24**, 946 (1991)]; RASTER3D [E. A. Merrit, M. E. P. Murphy, *Acta Crystallogr.* **D50**, 869 (1994)]; VMD [W. Humphrey, A. Dalke, K. Schulten, *J. Mol. Graphics* **14**, 33 (1996)]; MSMS [M. F. Sanner, J.-C. Spahn, A. J. Olson, *Biopolymers* **38**, 305 (1996)]; Matthews Coefficient [B. W. Matthews, *J. Mol. Biol.* **33**, 491 (1968)]; PROCHECK [R. A. Laskowski, M. W. MacArthur, D. S. Moss, J. M. Thornton, *J. Appl. Crystallogr.* **26**, 283 (1993)]; and O [T. A. Jones, J. Y. Zhou, S. W. Cowan, M. Kjeldgaard, *Acta Crystallogr.* **A47**, 110 (1991)].
46. We thank F. Bazan, W. Weis, and R. Kastelein for helpful discussions; J. Ho, J. Coller, and B. Opman for technical assistance; the staff of the Advanced Light Source (G. McDermott and T. Earnest); and the staff of the Stanford Synchrotron Radiation Laboratory (SSRL) (M. Soltis and P. Kuhn). Supported by a post-doctoral training grant (NIH) to the Department of Microbiology and Immunology (D.-c.c.), the California Cancer Research Program and American Heart Association (X.-L.H.), the Stanford Immunology Program (A.L.S.), and the Cancer Research Institute, the California Cancer Research Program, a Rita Allen Foundation award, NIH (grant RO1-AI-48540-01), and the Stanford University School of Medicine (K.C.G.). Coordinates are available from the Protein Data Bank (PDB) under accession code 111R. Coordinates of the tetramer are also available from the authors (kcgarcia@stanford.edu).

14 December 2000; accepted 6 February 2001